CrossMark

Phase control algorithms and filamentation of ultrashort laser pulses in a scattering medium

Simon Lefebvre[1] · Hakim Belmouaddine[1] · Denis Morris[2] · Daniel Houde[1]

Abstract

The scattering nature of biological systems restricts the non-linear propagation of coherent light in media of biological interest. Using a spatial phase shaping technique, we optimize the filamentation of femtosecond laser pulses in an ethanol solution containing a fluorescent dye, while the laser beam has first traveled through 1 cm of scattering aqueous solution. Following three-photon absorption process, the fluorescence signal of the Coumarin 440 dye is used as a control parameter by genetic and partitioning algorithms. Applied to the incident wavefront, the partitioning algorithm successfully enhances the dye fluorescence signal in a medium with a scattering coefficient (μ_s) varying from 1.24 to 3.71 cm^{-1} and gives rise to the production of a single laser filament several millimeters inside the observation cell that contains an ethanol solution. Interestingly, the optimal enhancement for the highest scattering medium is obtained with the partitioning algorithm at the lowest resolution. On the other hand, no significant enhancement is obtained when applying the genetic algorithm.

1 Introduction

Recent studies highlighted the effective action in a biological environment of radical oxygen species (ROS) produced "ex situ" by the generation of cold atmospheric plasma [1, 2]. An alternative approach has been recently introduced by Meesat et al. [3], where reactive species responsible for similar biological outcomes are generated directly "in situ" within the system of biological interest via laser-induced "cold" low density plasma. The non-linear propagation of femtosecond (fs) laser pulses in Kerr media can be harnessed to result in the production of cold plasma micro-channels, or filaments, via the filamentation of the corresponding laser beam [4, 5]. Inside a biological medium such as a tissue, the scattering of light, rather than the absorption, represent the principal obstacle to the non-linear propagation of fs laser pulses [6]. As for laser filamentation, scattering is responsible for a farther position of the non-linear focus, a shorter filament length and the apparition of a speckle structure in

the peripheral part of the beam which promotes the formation of multiple filaments [7]. Thus, the scattering spoils the main attribute granted to the laser irradiation which is the localization of the ROS production within the targeted volume of interest. In the present study, we explore an innovative approach to counterbalance the scattering to optimize the non-linear propagation of light towards the subsequent production of a single mono filament inside a diffusive media at a specific depth.

Modification of light propagation properties in an aqueous medium can be done by controlling the incident wavefront phase. Vellekoop et al. [8] applied this technique to enhance the intensity of forward scattered light at the output of the medium. They successfully increased the light intensity by 1000 times using a spatial light modulator together with feedback algorithms. A similar approach was used to successfully control the length and position of the laser filamentation in a non-diffusing medium (pure water) [9]. In addition, this technique also allowed to control the spatio-temporal extent of a pulsed laser beam [10, 11] and to optimize a fluorescence signal resulting from two-photon absorption process in a highly scattering medium, such as a thin slice of rat brain [12]. Similarly, a second harmonic generation signal enhancement has been obtained when this signal is used as an optimization parameter [13–15]. Recently, the application of wavefront

✉ Denis Morris
  Denis.Morris@USherbrooke.ca

1 Department of Nuclear Medicine and Radiobiology, Faculty of Medecine and Health Sciences, Université de Sherbrooke, Sherbrooke, QC J1H 5N4, Canada

2 Département de Physique, Faculté de Sciences, Université de Sherbrooke, Sherbrooke, QC J1K 2R1, Canada

shaping to three-photon microscopy led to an improvement of the signal for brain imaging [16, 17].

Pragmatic applications of the present light-induced treatment would primordially target the human skin. A hypothetical, practical scenario would ultimately consist in preserving the outer layer of the skin (epidermis), while restricting the biological effects of the generated ROS to the targeted volume, a few millimeters inside the underlying layers of the skin. With the objective of off-setting the detrimental effects induced by the scattering of the epidermis, the incident wavefront phase must be shaped accordingly. To this end, we studied the optimization of the non-linear propagation in a more fundamental approach. Here, the disturbance caused by the epidermis is simulated by the initial propagation of the laser pulses through a primary cell filled with a scattering solution. A 100 μm thick epidermis has a typical scattering coefficient (μ_s) of about 200 cm^{-1} at 800 nm (taking a reduced scattering coefficient (μ_s') of 20 cm^{-1} and an anisotropy factor of 0.9 from Refs. [18–20]). Accordingly, we used a 1 cm long primary cell filled with different solutions with scattering coefficients ranging from 1.24 to 3.71 cm^{-1}. The increased traveling distance in the diffusive cell compensate for its lower scattering coefficient.

The volume hosting the filaments is located downstream in a secondary cell acting as the underlying layers of skin. Since the epidermis is the most diffusive medium of the biological tissues, we neglected the scattering present in the underlying layers of the skin and used a non-diffusive solution to visualize the plasma micro-channel more easily. The fluorescence of a dye diluted in the corresponding solution, which was induced by multiphoton absorptions, accounted for the non-linear optical effects. Therefore, we used this fluorescence signal as the optimization parameter for our phase control algorithms.

This manuscript explores the impact of wavefront shaping with phase control algorithms on the propagation of femtosecond laser pulses in this two cells setup. Our goal is to establish a successful set of parameters for the algorithms that leads to the production of a single, stable filament inside the volume of interest, while the energy deposition is minimized in the scattering medium. To our knowledge, the present study represents the first attempt to implement wave front shaping technologies to counterbalance the effects of scattering on fs laser filamentation. Our results show that the different tested algorithms enhance the dye fluorescence signal, measured at 440 nm, as well as the supercontinuum signal, generated within a single filament and measured at 700 nm, in comparison with those obtained without any wavefront shaping. The influence of the scattering coefficients of our media on the figure of merit used in our optimization procedure is also discussed.

2 Materials and methods

2.1 Experimental setup

Our experimental setup is schematically shown in Fig. 1. The laser source (Spitfire ACE, Spectra-Physics) delivered 35 fs pulses of light centred at 800 nm at a repetition rate of 1 kHz. A half-wave plate and a polarizing cube beam splitter (not shown in Fig. 1) were used to control the intensity of the linearly polarized beam (s polarization) that is used for the experiments. The optical power, measured after the light diffuser cell, was fixed at 3.5 mW for all the experiments. The laser pulse duration was adjusted to produce the best filament in pure water (eye observation) and the corresponding pulse width was about 100 fs. The beam was expanded using a 2× telescope to cover most of the active area of the SLM device (LCOS-SLM, model X10468-02 from Hamamatsu). The SLM's output beam was then loosely focused into a series of two cells, separated by 10 cm: the first one designated as the light diffuser cell and the second one designated as the observation cell (see below for details). The focal length of the first lens (L_1) is 75 cm. Distances between the lens and the two cells were adjusted such that the focal point of the lens was located in the middle of the observation cell. The different light signals correspond to fundamental wave at 800 nm, the dye fluorescence emitted around 440 nm and the supercontinuum light generated within the laser filament (detected at 700 nm). These light beams coming from a chosen zone in the observation cell were then imaged with a 1.6× magnification onto a CCD Camera (Nikon D810, 24 × 36 mm, 7360 × 4192 pixels, RGB) using a pair of lenses (L_2 and L_3) with focal lengths of 25 cm and 40 cm, respectively. The position of L_2 lens was adjusted to image different zones along the laser beam path. Depending
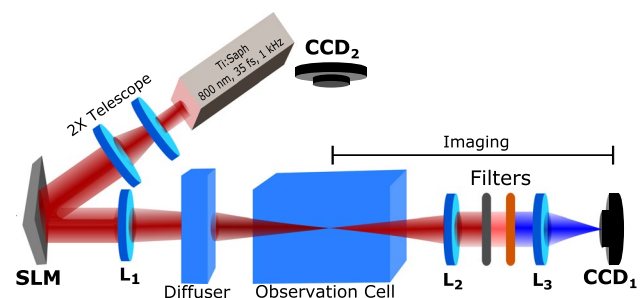

Fig. 1 Experimental setup used to study laser filamentation after the passage through a light diffuser cell. Camera CCD$_2$ is used to visualize the lateral profiles of the laser beam, through its propagation in the observation cell. Camera CCD$_1$ is used to visualize the different light control signals emitted from a chosen area located in the observation cell. The lenses L_1, L_2, L_3 have focal lengths of 75, 25 and 40 cm, respectively. The imaging arm contains optical attenuators and a bandpass filter centred on the emission wavelength of the light signal of interest

on the light signal to be measured, attenuators and bandpass filters were used to enhance the image contrast. A second CCD camera was also used to observe lateral scattering light along the laser beam path inside the observation cell. These lateral images of the beam were obtained without filters in front of the CCD camera. The images of the lateral scattering light were taken with an exposure time of 100 ms, while the images of the other light signals, obtained in the forward direction, were taken with an exposure time of 10 or 20 ms.

The 1 cm long light diffuser cell was filled with either pure water for control or an aqueous suspension of polystyrene microspheres, calibrated at a diameter of 1.7 μm (Vasmo Inc). The concentration of these suspensions were 15,000, 30,000 and 45,000 particles mm^{-3}, corresponding to a scattering coefficient (μ_s) of 1.24, 2.47 and 3.71 cm^{-1}, respectively. Scattering coefficients were determined by simulation of Mie scattering theory by the Oregon Medical Laser Center [21]. The light power that can be tolerated by the SLM device sets the maximum value of opacity of the scattering medium.

The 4 cm long observation cell was filled with an ethanol solution containing a concentration of 1.25 ng ml^{-1} of fluorescent dye (Coumarin 440). This dye can be excited via three-photon absorption mechanism due to a broad absorption band centred at 350 nm [22]. On the other hand, the first electronic absorption threshold in liquid ethanol is 6.9 ± 0.1 eV [23]: the five-photon absorption mechanism is therefore required to initiate the plasma formation. Considering a non-linear refractive index of $n_2 = 2.6 \times 10^{-16}$ cm^2 W^{-1}, the critical power for self-focusing leading to the laser filamentation process is about 3.0 MW in ethanol [24]. As mentioned by Schroeder and Chin [25], adding a low dye concentration in the ethanol solution has no significant impact on the light propagation properties and filamentation dynamics.

2.2 Random matrix theory and DMPK equation

Scattering processes can be described statistically using the random matrix theory (RMT) and the more refined DMPK approach [26], which considers the thickness of the medium as well as the mean free path. When considering many transverse channels, the DMPK equation predicts three specific scattering regimes: ballistic, diffusive and localized. The ballistic regime takes place in a weak scattering medium when the system length is smaller than the mean free path. The localized regime is established in a strong scattering medium when the system length is larger than the "localization length" [27]. For the intermediate case, the transmission of photons in the diffusive regime is characterized by a distribution of transmission channels described by the following distribution function [28]:

$$P(\tau) = \frac{Nl^*}{2L} \frac{1}{\tau \sqrt{1-\tau}}, \tag{1}$$

where N is the total number of transmission channels, l^* is the mean free path, L is the system length and τ is the transmission coefficient. This distribution is illustrated in Fig. 2.

One surprising result of the RMT approach is that the transmission channels are not uniformly distributed between the limiting values of the transmission coefficient (0 and 1). Instead, the model predicts that most channels correspond to either an open channel (total transmission) or a closed channel (zero transmission). This bimodal distribution of transmission channels will be useful to analyze our results.

2.3 Optimization procedure

The SLM was divided in N equally sized square segments. Resolutions of $N = 48, 192, 300, 768$ and 1200 individually controlled segments were used to maximize the dye fluorescence signal at a specific depth inside the observation cell. A total of 10 degrees of freedom were used for pixel voltages on the SLM, limiting the phase shift to a resolution of $\pi/5$.

For every wave shaping experiments, the following procedure was used. First, all pixels of the SLM were initialized at the same voltage, corresponding to a $\pi/2$ flat phase pattern. With the movable L_2 lens, we then scanned around the geometrical focus inside the observation cell to find a zone of high dye fluorescence. The averaged forward scattering image, obtained from 5 to 15 images captured with the initial phase mask, corresponds to our reference for the non-optimized filamentation profile. The onset of fluorescence of the Coumarin 440 was correlated with the onset of laser filamentation by detecting the light intensity at different wavelengths: 440 nm for the dye fluorescence and 700 nm for the supercontinuum generated within the filament. The light intensity profile detected at 800 nm was also used as an indicator of the energy distribution within the primary fundamental laser beam. Second, either an iterative partitioning algorithm [29] or a genetic algorithm [30] was used to select the SLM phase mask at each step of the optimization loop (see details below). These phase masks, corresponding to a series of voltages applied to the different pixels of the SLM, act on the wavefront of the laser beam and affect the three-photon absorption mechanism responsible for the dye fluorescence. For every phase mask created by the algorithms, an image of the resulting fluorescence inside the observation

Fig. 2 Distribution of transmission channels with coefficient τ for a diffusive scattering medium, given by Eq. (1). Image taken from [28]
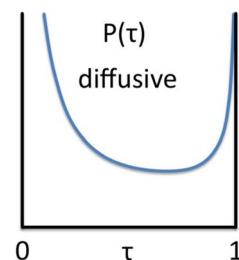
cell was taken by the CCD Camera. Every pixel of the image was converted to a greyscale value with a chosen intensity level given by: $I = 0.05R + 0.05G + 0.90B$, where R, G and B correspond to the intensities measured in the red, green and blue part of the spectrum, respectively. The converted greyscale values were used to assign a figure of merit (FOM) to that specific phase mask. The FOM value is calculated using this formula [31]:

$$FOM = \sum_{\substack{i,j \\ x_i \neq x_0, \ y_j \neq y_0}} \frac{I_{ij}}{\left(\sqrt{(x_i - x_0)^2 + (y_j - y_0)^2} \right)^n} \quad (2)$$

where I_{ij} is the gray scale intensity for each pixel (i,j) of the 2D image, x_0 and y_0 are the coordinate points of the central part of the optimization target and the exponent n is a power factor, giving higher weighting to pixels closer to the optimization target. In our experiment, we used $n = 8$ to offer a better distinction between a localized intense fluorescence spot and a weak and diffuse speckle spot. Iterative algorithms used the FOM associated with each phase mask as feedback for optimization. For the partitioning algorithm, an average of 70 iterations, lasting approximately 45 min, were needed to optimize the fluorescence signal emitted by Coumarin 440, while 200 iterations and 2 h were required for the genetic algorithm.

The iterative partitioning algorithm was selecting phase masks by incrementally adjusting the phase shift of a randomly selected population, which consisted of half of the total segments used. At the end of the phase cycle, the best phase shift was attributed to each segment and a new population was randomly selected for the next iteration. The algorithm was tested for five different resolutions ($N = 48, 192, 300, 768$ and 1200), for different scattering coefficients of the light diffusive medium.

For the genetic algorithm, an initial random population of phase masks was optimized with the creation of offspring by combining the characteristics of two parents from the population and allowing mutations. Every segment of the new offspring phase mask had a chance R to be mutated, namely being attributed a random phase shift, given by [30]:

$$R = \left(R_0 - R_{end} \right)^{-n/\lambda} - R_{end} \quad (3)$$

where n is the number of iterations performed, R_0 and R_{end} are the initial and final mutation rates, and λ is the mutation rate decay factor. Values of parameters chosen for this study are displayed in Table 1. The initial number of individually controlled segments (resolution N) is 48. As the population narrows to a positive solution, the resolution was gradually increased during the optimization process.

At the end of each experiment, the optimized fluorescence profile was determined by averaging 5–15 images

Table 1 Parameters for the genetic algorithm

Population size	20
New offspring per generation	10
Initial mutation rate (R_0)	0.1
Final mutation rate (R_{end})	0.015
Mutation rate decay factor (λ)	400
Resolution (N)	$48 \rightarrow 1200$

of the forward scattering light and then applying the FOM equation (Eq. 2); while the possible error on the FOM value was estimated from the standard deviation of the population. Comparison between the populations of images that led to the optimized profile and the population for the non-optimized profile were done with a Student's T test and significant differences were found with $p < 0.005$ as criteria. Enhancement is calculated with the ratio of optimized FOM value over the non-optimized FOM value for this particular scattering medium.

3 Results

The lateral intensity profile of the non-optimized pulsed laser beam, through its propagation in the aqueous medium of the observation cell, is shown in Fig. 3a. These results were obtained for a light diffuser cell medium having a scattering coefficient of 1.24 cm^{-1}. The light signal corresponding to the fluorescence of Coumarin 440 and emitted from a specific region inside the observation cell was imaged in the forward direction on a CCD camera (see Fig. 1 for details). The filtering of other wavelengths was obtained using a 450 ± 20 nm bandpass filter. Three specific regions of higher fluorescence were evidenced along the laser beam path. Images of the fluorescence emitted from these regions (equivalent to sectional views) are shown above the lateral intensity profile of the beam.

We then tried to correlate the above fluorescence images with those coming from other light signals characteristic of the formation of a laser filament, namely the light present in the fundamental wave (energy reservoir) and that associated with the supercontinuum generation. Images of forward scattered light at 800 nm and from part of the supercontinuum generated at 700 nm are obtained using 800 ± 5 nm and 700 ± 5 nm bandpass filters, respectively. Results showed no supercontinuum generation in the first high fluorescence zone. This suggests that the electric field was not strong enough to cause plasma formation at this position. The supercontinuum generation signal started to rise at the end of the second high fluorescence zone, as shown in the second 700 nm image (see Fig. 3a). The spatial separation (about 3 mm) between these zones was related to the different light
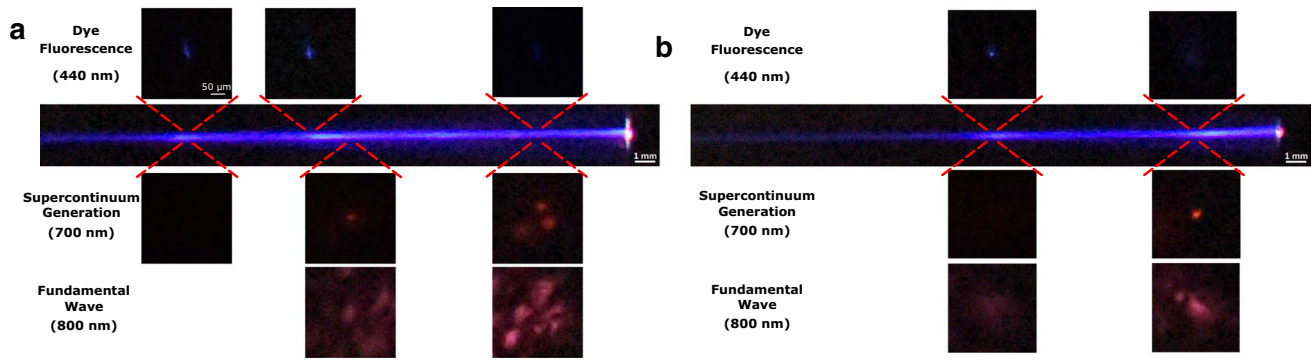
Fig. 3 The central images correspond to lateral intensity profiles of the laser beam, through its propagation in the observation cell, **a** before and **b** after pulse shaping of the incident beam wavefront on a light diffuser cell characterized by a scattering coefficient (μ_s) of 1.24 cm^{-1}. Images of the different light control signals (dye fluorescence, supercontinuum and fundamental wave) emitted from a specific region (marked in red), and detected in the forward direction, are shown above and below the images of the lateral beam profiles

intensity thresholds required to trigger the two phenomena, namely the three-photon dye absorption process and the plasma formation via five-photon absorption mechanism. The corresponding image of the forward scattering light at 800 nm, observed at the position where the generation of a supercontinuum began, shows a broad central spot surrounded by several other diffuse speckle spots. This image suggests that the scattering medium tends to redistribute the energy contained in the primary beam between several other beams of lower intensity. This phenomenon can lead to the formation of multiple laser filaments. This was actually observed few millimeters away in the observation cell, at the position of the third high fluorescence zone. Indeed, three distinct spots were observed in the image of the supercontinuum detected at 700 nm. Moreover, the image of the transverse intensity distribution of the fundamental wave at 800 nm still presented several diffuse spots.

Figure 3b shows the results obtained after wavefront shaping of the incident wave on the scattering medium. The images of the different light signal were obtained after optimization of the phase masks using an iterative partitioning algorithm with a resolution of $N = 768$. Based on the results obtained for the non-optimized wavefront, the intensity profile at the second strong dye fluorescence zone (where the laser filament was just about to appear) was chosen as the light control signal for the optimization procedure. It is interesting to mention that the first high dye fluorescence zone, observed for the non-optimized case, has completely disappeared. As expected, the dye fluorescence intensity profile of the selected control zone (the middle of the observation cell) shows a strong and unique spot. Moreover, the intensity profile corresponding to the light scattered at 800 nm reveals a relatively large spot but no sign of subdivision of the primary beam. The intensity profile seen in the image of the light detected at 700 nm shows no signature of a supercontinuum generation at this

position. These results suggest that the energy threshold for laser filamentation is still not reached at the position where the dye fluorescence intensity is stronger. Finally, the supercontinuum signal appears approximately 7.5 mm away from the position of the control signal zone. The weak dye fluorescence signal at this position remains unclear, but the ionization of the medium seems to be detrimental to the multiphoton dye absorption processes. Our results indicate that more energy of the fundamental wave is directed towards non-linear effects of higher order. The phase mask optimization procedure is effectively producing a single laser filament in the observation cell. The intensity profiles of the fundamental wave at 800 nm, detected at different positions along the laser beam path, showed a much more symmetric distribution of the energy, compared to the non-optimized case.

Knowing that the control signal from the dye fluorescence, emitted in the central zone of the observation cell, can effectively be used to optimize the production of a single laser filament, we then sought to study the impact of the scattering coefficient of the diffuser cell medium on this control signal used by phase control optimization algorithms. The results of this study are summarized in Fig. 4. The non-optimized and optimized averaged fluorescence profiles obtained for different scattering coefficients of the diffusive medium, ranging from 0 to 3.71 cm^{-1}, are displayed in Fig. 4a. A total of 5–15 images were averaged to obtain each profile. The FOM values (see Eq. 2) of each image are regrouped in the corresponding histogram (Fig. 4b). The numbers 48, 192, 300, 768 and 1200 correspond to the resolution selected for the partitioning algorithm. For the genetic algorithm, the best fluorescence profile was selected among the three best masks of the population at the end of the optimization procedure and then averaged using a population of images. In most cases, the optimization procedure succeeded to improve the figure of merit of the dye fluorescence profile
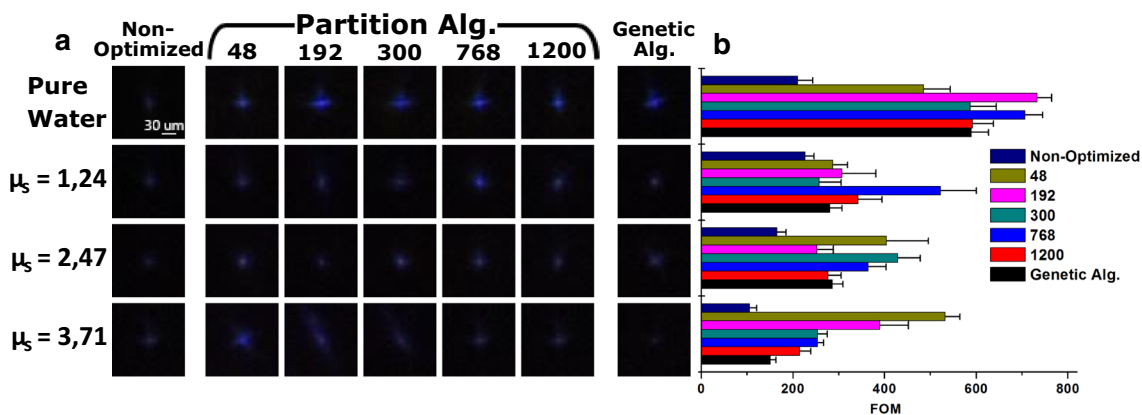
Fig. 4 a Set of averaged dye fluorescence images obtained before (non-optimized) and after pulse shaping of the incident wavefront. Results obtained with the partitioning and the genetic phase control algorithms are compared, for different media characterized by their scattering coefficient (μ_s). **b** Histogram of the figure of merit values (calculated using the fluorescent profile with Eq. 2) obtained for each medium. The numbers 48, 192, 300, 768 and 1200 correspond to the resolution selected for the partitioning algorithm. Uncertainties come from the standard deviation of the population of images

and gave rise to the production of a single filament, produced a few millimeters deeper in the observation cell.

When comparing the averaged FOM value of optimized and non-optimized fluorescence profiles (Fig. 4b) in a non-scattering media (pure water), a significant ($p < 0.005$) difference was found for every experimental conditions. The optimization procedure led to an increase in fluorescence signal by 2.3–3.5 times when compared to the essay done without wavefront shaping. For the lowest scattering media ($\mu_s = 1.24$ cm^{-1}), a significant difference was found for each experiment, except two that was carried out by the partitioning algorithm with a resolution of $N = 192$ and $N = 300$. The best improvement by 2.3 times was obtained with a resolution of $N = 768$. For the second scattering media ($\mu_s = 2.47$ cm^{-1}), all resolutions gave rise to a significant improvement; the best enhancement (2.5 times) was obtained with $N = 300$. Regarding the highest scattering media ($\mu_s = 3.71$ cm^{-1}), the optimal improvement was obtained with $N = 48$. It is noteworthy that the best improvement (5.0 times) using our partitioning algorithm was obtained for the highest scattering medium combined with the lowest resolution. Taken together, the partitioning algorithm has successfully increased the dye fluorescence signal when compared across all different scattering media, while the genetic algorithm partially increased the dye fluorescence signal, only in the lowest and second scattering media.

Also, when comparing the non-optimized FOM values across the different scattering media, the initial fluorescence intensity decreases with an increase in scattering coefficient. It is an expected phenomenon, as fewer ballistic photons are available to contribute to the fluorescence intensity at the focal point as the scattering regime increases. While the overall enhancement also increases with the scattering regime, this is mostly due to the lower fluorescence intensity of the non-optimized profile in a high scattering media. The strong enhancement of the FOM value is expected because the fluorescence intensity is extremely low after the passage of the laser beam through this light diffuser cell.

4 Discussion

After optimization by phase control algorithms, the expected enhancement for a linear signal such as optical intensity is directly proportional to the number of input modes (N) on the SLM [8]. Intuitively, we expected that an increase in the phase mask resolution, used by the partitioning algorithm, would lead to a greater enhancement of the dye fluorescence control signal. However, our results suggest that this is not always the case and that it would be more desirable to adjust the number of input modes to the scattering coefficient of the medium.

To explain this discrepancy, we will look at the distribution of transmission channels, first presented in Sect. 2.2, for every scattering media. In a practical case, such as the loss of non-waveguide situation of light propagation in a random scattering medium, the transmission matrix components are no longer correlated (i.e., unitary). In this case, the bimodal distribution of transmission channels (Eq. 1) takes the form of a quarter circle distribution [32]:

$$P(T) = \frac{4}{R^2\pi}\sqrt{(R^2 - T^2)} \quad (0 \le T \le R) \quad (4)$$

where $R = 3\pi/4\langle T\rangle$. Defining the average transmission $\langle T\rangle$ as the ratio of transmitted optical power across the scattering medium, a distribution of possible transmission channels are found for each scattering media, which is presented in

Fig. 5. We no longer have a bimodal distribution of possible transmission coefficient (0 and 1); instead, we found, on average, a high probability of finding a low efficiency channel and a low probability of finding a high efficiency channel. In pure water, since the ratio of power transmitted is high, there is a large distribution of channels with transmission coefficient as high as 0.6. Since there are no scatterers to disrupt the incident wavefront, the optimized FOM values are higher due to the existence of high efficiency channels which leads to a great improvement (2.3–3.5 times) over the non-optimized case.

Across all media, the genetic algorithm had a lower FOM enhancement than most of the experiments done with the partitioning algorithm. In addition to the much longer time needed to reach a satisfactory solution, the genetic algorithm has trouble when there is a very low or no signal at the beginning of the experiment. Once at least half of the mask population reaches a moderate signal, then the genetic algorithm can achieve a level of enhancement on par with the partitioning algorithm, as demonstrated in pure water. Due to the random nature of its approach, it must randomly find an optimal phase pattern that unlocks an open channel inside the scattering medium. If the initial random population of phase masks and subsequent offspring all give similar levels of signal, there is not enough variation between the mask population and the newly generated offspring to drastically change the phase pattern and find an open channel. Since the number and probability of finding an open channel decrease as the scattering coefficient increases, the genetic algorithm was only able to reach a satisfactory solution once, in pure water, where the number of high efficiency channels were higher. In a scattering medium, a different population size and mutation rates may result in better enhancements.
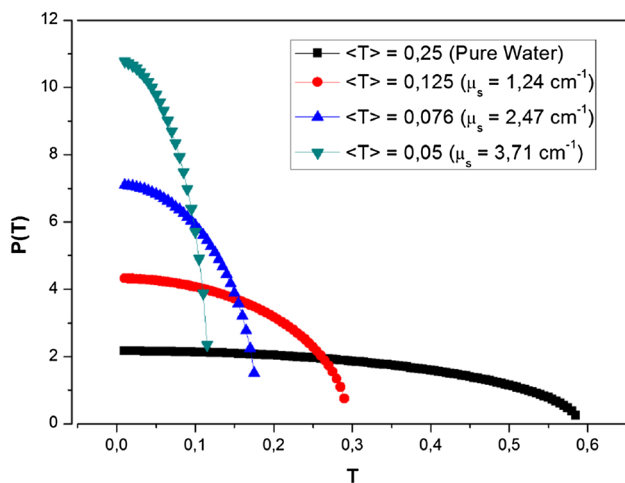

Fig. 5 Distribution of transmission channels $P(T)$ (Eq. 4) for different values of average transmission $\langle T \rangle$ corresponding to our scattering media

As the scattering coefficient increases from 1.24 to 3.71 cm^{-1}, the optimized FOM values decrease, which suggest that the optimization procedure is less efficient in a high scattering regime. When considering the distribution of transmission channels for these scattering media (Fig. 5), the number and efficiency of open channels decrease as the scattering coefficient increases. Since it is more efficient to find open channels for a significant improvement in transmitted optical power to occur, it follows that the overall improvement must decrease as the efficiency and probability of open channels decrease.

Finally, when considering the best optimized FOM value and its resolution for each scattering media, we found that the best enhancement (2.3 times) for the lowest scattering medium was achieved with a high resolution ($N = 768$), while the best enhancement (5.0 times) for the highest scattering medium was achieved with a low resolution ($N = 48$). In light of the distribution of open and closed channels associated with these scattering media, it seems that phase masks with a higher resolution are more efficient when precisely adjusting the wavefront to find an open channel, of which there were more in the low scattering medium. On the other hand, when low-resolution phase masks are used, the optimized phase pattern seeks to maximize the contribution of multiple low efficiency channels. In this case, finely tuning the phase masks with a higher resolution did not result in finding an open channel, as evidenced by the lower enhancement obtained with high-resolution phase masks in the highest scattering media.

In light of these results, it is clear that the enhancement for three-photon absorption mechanism is not directly proportional to the number of modes on the SLM. Furthermore, when the scattering media is very diffusive, phase optimization with a low-resolution phase mask will yield better results than with a high-resolution one. To achieve the highest enhancement possible, it would be more desirable to adjust the number of input modes to the scattering coefficient of the medium.

5 Conclusion

We have investigated the action of phase control algorithms on the generation of a single filament when the beam has to travel through a scattering medium. Using iterative optimization of the incident wavefront with partitioning and genetic algorithms, the fluorescence from three-photon absorption process in a Coumarin 440 dye was used as the optimization parameter. Results show an enhancement of the dye fluorescence signal after optimization as well as the formation of a single filament a few millimeters inside the observation cell. In the case of three-photon absorption process, results also show that the number of input modes on the SLM is not

linearly correlated with the expected enhancement. Lastly, the reason why the best enhancement was achieved with the lowest resolution in the highest scattering medium is explained when considering that a low-resolution optimization maximizes the overall contribution of closed channels, while a high-resolution optimization maximizes the efficiency of a single open channel. The differences in the distribution of open and closed channels for the different scattering media have an impact on the best SLM's resolution to choose to optimize the light control signal through wavefront shaping and phase control algorithms.

A low-resolution partition algorithm appears conducive to optimize the non-linear propagation of the fs laser pulses in an ethanol solution with a scattering coefficient of 3.71 cm^{-1}. Nevertheless, it is important to note that the average scattering coefficient for a biological tissue such as the human skin is around 200 cm^{-1} at 800 nm. Our ultimate goal is to further advance towards the optimization of the fs laser filamentation in a much more concrete biological environment. To do so, future works intend to implement such phase control algorithms within the much more realistic framework of the non-linear propagation of light in a thin slice of biological tissue. Furthermore, the feedback signal acquired from an image of the forward scattered light would not be accessible in a practical situation. Promising new and non-invasive feedback or conjugation guidestars such as photo-acoustic detection [33] allow the retrieval of information about light intensity within a biological media. Although these technologies are conventionally used with monochromatic light, it would be interesting to study their impact on femtosecond pulses and the resulting filamentation profile in scattering media.

Compliance with ethical standards

Conflict of interest The authors declare that they have no conflict of interest. The authors would like to thank Benoît Paquette for helpful comments.

References

1. M. Chatraie, G. Torkaman, M. Khani, H. Salehi, B. Shokri, Sci. Rep. **8**, 5621 (2018)
2. C. Schneider, L. Gebhardt, S. Arndt, S. Karrer, J.L. Zimmermann, M.J.M. Fischer, A.-K. Bosserhoff, Sci. Rep. **8**, 10048 (2018)
3. R. Meesat, H. Belmouaddine, J.-F. Allard, C. Tanguay-Renaud, R. Lemay, T. Brastaviceanu, L. Tremblay, B. Paquette, J.R. Wagner, J.-P. Jay-Gerin, M. Lepage, M.A. Huels, D. Houde, Proc. Natl. Acad. Sci. USA **109**, E2508 (2012)
4. A. Couairon, A. Mysyrowicz, Phys. Rep. **441**, 47 (2007)
5. S.L. Chin, *Femtosecond Laser Filamentation* (Springer, New York, 2010), p. 130
6. H. Yu, J. Park, K. Lee, J. Yoon, K. Kim, S. Lee, Y. Park, Curr. Appl. Phys. **15**, 632 (2015)
7. V. Jukna, G. Tamošauskas, G. Valiulis, M. Aputis, M. Puida, F. Ivanauskas, A. Dubietis, Appl. Phys. B **94**, 175 (2007)
8. I.M. Vellekoop, A.P. Mosk, Opt. Lett. **32**, 2309 (2007)
9. G. Heck, J. Sloss, R.J. Levis, Opt. Commun. **259**, 216 (2006)
10. O. Katz, E. Small, Y. Bromberg, Y. Silberberg, Nat. Photon. **5**, 372 (2011)
11. D.J. McCabe, A. Tajalli, D.R. Austin, P. Bondareff, I.A. Walmsley, S. Gigan, B. Chatel, Nat. Commun. **2**, 447 (2011)
12. O. Katz, E. Small, Y. Guan, Y. Silberberg, Optica **1**, 170 (2014)
13. J. Aulbach, B. Gjonaj, P.M. Johnson, A.P. Mosk, A. Lagendijk, Phys. Rev. Lett. **106**, 103901 (2011)
14. Y. Qiao, Y. Peng, Y. Zheng, F. Ye, X. Chen, Opt. Lett. **42**, 1895 (2017)
15. J.V. Thompson, B.H. Hokr, G.A. Throckmorton, D. Wang, M.O. Scully, V.V. Yakovlev, ACS Photon. **4**, 1790 (2017)
16. X. Tao, J. Lu, T. Lam, R. Rodriguez, Y. Zuo, J. Kubby, Neural Imaging Sens. SPIE Proc. **10051**, 100510R (2017)
17. D. Sinefeld, H.P. Paudel, T. Wang, M. Wang, D.G. Ouzounov, T.G. Bifano, C. Xu, Adapt. Optics Wavefront Control Biol. Syst. III SPIE Proc. **10073**, 1007314 (2017)
18. S.L. Jacques, Phys. Med. Biol. **58**, R37 (2013)
19. A.N. Bashkatov, E.A. Genina, V.V. Tuchin, J. Innov. Opt. Health Sci. **4**, 9 (2011)
20. E. Salomatina, B. Jiang, J. Novak, A.N. Yaroslavsky, J. Biomed. Opt. **11**, 064026 (2006)
21. S. Prahl, Mie Scattering Calculator. http://omlc.org/calc/mie_calc.html
22. U. Brackmann, *Lambdachrome Laser Dyes*, 1st edn. (Lambda Physik GmbH, Göettingen, 1986), p. III-59
23. J.M. Jung, Chem. Phys. Lett. **366**, 67 (2002)
24. L. Guyon, K.M. Hajek, F. Courvoisier, V. Boutou, R. Nuter, A. Vinçotte, S. Champeaux, L. Bergé, J.-P. Wolf, App. Phys. B **90**, 383 (2008)
25. H. Schroeder, S.L. Chin, Opt. Commun. **234**, 399 (2004)
26. O.N. Dorokhov, JETP Lett. **36**, 318 (1982)
27. P.W. Anderson, Phys. Rev. **112**, 1900 (1958)
28. S. Rotter, S. Gigan, Rev. Mod. Phys. **89**, 015005 (2017)
29. I.M. Vellekoop, A.P. Mosk, Opt. Commun. **281**, 3071 (2008)
30. D.B. Conkey, A.N. Brown, A.M. Caravaca-Aguirre, R. Piestun, Opt. Express **20**, 4840 (2012)
31. Z.-H. He, B. Hou, V. Lebailly, J.A. Nees, K. Krushelnick, A.G.R. Thomas, Nat. Commun. **6**, 7156 (2015)
32. S.M. Popoff, G. Lerosey, R. Carminati, M. Fink, A.C. Boccara, S. Gigan, Phys. Rev. Lett. **104**, 100601 (2010)
33. R. Horstmeyer, H. Ruan, C. Yang, Nat. Photon. **9**, 563 (2015)